Journal of Magnetic Resonance 276 (2017) 86–94

Contents lists available at ScienceDirect

Journal of Magnetic Resonance

journal homepage: www.elsevier.com/locate/jmr

Time-domain shape of electron spin echo signal of spin-correlated radical pairs in polymer/fullerene blends

Alexander A. Popov [a,b,*], Ekaterina A. Lukina [a,b], Leonid Rapatskiy [c], Leonid V. Kulik [b,a]

[a] Novosibirsk State University, Pirogova 2, Novosibirsk 630090, Russia
[b] Voevodsky Institute of Chemical Kinetics and Combustion of the Siberian Branch of the Russian Academy of Sciences, Institutskaya 3, Novosibirsk 630090, Russia
[c] Max Planck Institute for Chemical Energy Conversion, Stiftstrasse 34 - 36, D - 45470 Mülheim an der Ruhr, Germany

ARTICLE INFO

Article history:
Received 24 August 2015
Revised 22 December 2016
Accepted 19 January 2017
Available online 23 January 2017

Keywords:
Pulsed EPR
Spin-correlated radical pairs
P3HT
PCBM
Interspin distance measurement

ABSTRACT

Temporal shape of electron spin echo (ESE) signal of photoinduced spin-correlated radical pairs (SCRP) in composite of conductive polymer P3HT and substituted fullerene PCBM is studied in details. ESE signals of radical pairs (RP) $P3HT^+/PCBM^-$ are calculated in realistic model, taking into account finite microwave pulse length. Inhomogeneous broadening of resonant lines and interradical distance distribution are included. Experimentally observed ESE time-domain shape was found to contradict predictions of conventional SCRP theory, which would be valid in the case of very fast electron transfer. Thus, instantaneous formation of singlet SCRP is not the case for $P3HT^+/PCBM^-$ pair, and spin system has enough time to evolve coherently during sequential electron transfer. While it is impossible to reproduce experimental data within simple singlet SCRP model, assumption of presence of additional – with respect to what is predicted by singlet SCRP theory – AE (absorption/emission) spin polarization gives convincing accordance with the experiment. Density matrix of RP $P3HT^+/PCBM^-$ is a superposition of two contributions, namely the parts reflecting (i) antiphase polarization of original singlet-born SCRP and (ii) additional AE-polarization which is generated during initial stage of charge separation. AE-polarization affects experimental ESEEM (electron spin echo envelope modulation) traces, as well as ESE shape, making impossible their interpretation via simple singlet SCRP model. However, this effect can be eliminated by averaging of ESEEM traces over EPR spectral positions. Finally, choosing the optimal gate for ESE time-domain integration and proper microwave detection phase tuning are considered.

1. Introduction

Polymer/fullerene blend is the most widely used active media for organic photovoltaics (OPV) devices. The power conversion efficiency (PCE) of OPV cells is determined, to the large extent, by the yield of photoinduced charge separation. For many polymer/fullerene blends, including the benchmark composite of poly(3-hexylthiophene) (P3HT) and [6,6]-phenyl-C_{61}-butyric acid methyl ester (PCBM), this yield is close to unity [1,2]. However, the origin of such a high efficiency of charge separation is still unclear, despite numerous studies [3,4]. The main reason for this is lack of information about the structure and dynamics of the intermediates of charge separation at polymer/fullerene interface. These intermediates are usually called light-induced primary charge-separated (CS) states [5] or charge-transfer states (CTS) [6,7]. To determine the mechanism of charge separation in polymer/fullerene (or, more generally, in donor/acceptor) composites, knowledge of the distance between charges in CTS is needed. Since CTS can be caught at low temperature, when the charge separation is slowed down, EPR becomes a suitable method to study CTS structure.

Initially, CW EPR spectrum of separated charges in continuously illuminated polymer/fullerene composites were obtained [8]. This experiment proved the efficiency of light-induced charge separation in polymer/fullerene composites. However, lack of temporal resolution limits CW EPR experiments severely, and only thermalized separated charges are accessible for this method. Later, time-resolved (TR) EPR spectra were obtained for CTS in polymer/fullerene composite [5–7,9,10] under pulse laser illumination. It was established that light-induced CTS in P3HT/PCBM composite is spin-correlated radical pair (SCRP), consisting of two weakly interacting radicals (polarons) $P3HT^+$ and $PCBM^-$, created in the singlet spin state upon exciton dissociation. However, because of limited data set and complexity of the system the interpretation of TR EPR spectra is ambiguous.

* Corresponding author at: Novosibirsk State University, Pirogova 2, Novosibirsk 630090, Russia.
E-mail addresses: popov@kinetics.nsc.ru (A.A. Popov), katyaluk@yandex.ru (E.A. Lukina), leonid.rapatskiy@gmail.com (L. Rapatskiy), chemphy@kinetics.nsc.ru (L.V. Kulik).

http://dx.doi.org/10.1016/j.jmr.2017.01.016
1090-7807/

Electron spin echo (ESE), in particular, out-of-phase (OOP) ESE can provide more detailed information about the electronic structure of this SCRP [11]. Previously, this technique was successfully used to determine the structure of the intermediates of light-induced charge separation in bacterial photosynthetic reaction centers (RCs) [12–14] and plant photosystems [13]. For these systems out-of-phase ESE gives the unique possibility to determine the interspin distance in SCRP in nanometer range with angstrom precision. This distance nearly coincides with the distance between electron donor and acceptor molecules of RC, determined from X-ray structure [12,15]. Lately, out-of-phase ESE was used to study intramolecular light-induced charge transfer in artificial donor-spacer-acceptor systems [16,17].

Recently, out-of-phase ESE spectroscopy was employed for polymer/fullerene composites [18,19]. It was shown experimentally that time-domain shape of OOP ESE signal in P3HT/PCBM composite is nearly antisymmetric having negative and positive parts. At the same time OOP ESE signal in photosynthetic RCs, obtained under similar conditions [20], is bell-shaped, the signal sign is the same in every point and its maximum is well defined. Therefore, while obtaining electron spin echo envelope modulation (ESEEM) signal is straightforward in the case of RCs, it becomes tricky and ambiguous for the case of P3HT/PCBM composite: it is not clear how to derive properly ESE intensity upon time-domain integration in the latter case. Result of ESEEM experiment, being critical for interradical distance measurement, depends significantly on choice of integration interval of ESE signal.

There is another pitfall that is worth to point out. Interpretation of ESEEM data in the frame of SCRP theory is based on well known analytic expression for ESE modulation frequency [21]. Nevertheless, unusual time-domain ESE shape, obtained for radical pairs (RP) in P3HT/PCBM composite, makes questionable applicability of the SCRP theory for such systems. Thus, ESE data for RPs in polymer/fullerene composites cannot be interpreted in strictly the same way, as it was done for photosynthetic SCRP.

This work is devoted to systematic study of ESE signal in SCRP $P3HT^{+}/PCBM^{-}$ by numerical simulation of spin dynamics. The aim is to check whether the predictions of SCRP theory, which are valid for photosynthetic SCRP [21], are also valid for SCRP in polymer/fullerene composites. We analyzed the time-domain shape of ESE and derived the recommendation for choosing the interval for ESE integration in ESEEM experiments. Finally, the predictions of SCRP theory and results of ESE experiments with P3HT/PCBM under laser flash illumination are compared. We found that it is impossible to reproduce ESE time-domain shape and ESEEM data within the framework of conventional singlet SCRP theory. In order to explain this discrepancy we assume additional spin polarization to be generated at initial steps of photoinduced charge separation. Thus, spin state of $P3HT^{+}/PCBM^{-}$ RPs differs from pure singlet. We will call RPs, which carry this additional polarization, *AE-polarized*. The polarization itself is named, accordingly, *AE-polarization*. Individual radicals, which AE-polarized RP is composed from, carry net polarization, whether absorptive (A) or emissive (E), of opposite sign and the same magnitude. The origin of AE-polarization is coherent evolution of RP spin state prior to ESE experiment.

2. Theory and calculation method

The spin-Hamiltonian of a radical pair in the high-field approximation ($J, D \ll \mu g B_0$ for both spins) can be written as

$$\mathcal{H}_{\text{lab}} = \mu g_A B_0 S_{Az} + \mu g_B B_0 S_{Bz} + J(\mathbf{S}_A \cdot \mathbf{S}_B) + \frac{D}{2}(3\cos^2\theta_D - 1)\left(S_z^2 - \frac{1}{3}\mathbf{S}^2\right). \quad (1)$$

Here spin operators of radicals are denoted as $\mathbf{S}_i$ ($i = A, B$), $\mathbf{S} = \mathbf{S}_A + \mathbf{S}_B$, μ is a Bohr magneton, B_0 represents strength of the magnetic field, J and D are the values of exchange and dipolar interaction correspondingly, θ_D is an angle between line connecting spins and direction of the external magnetic field $\mathbf{B}_0$ and, finally, g_A and g_B denote effective g-factors of two species in radical pair. In Hamiltonian (1) we omit possible nonaxiality of dipole interaction tensor and use point-dipole approximation. The Hamiltonian (1) does not contain hyperfine interactions because number of interacting nuclei is too large. Instead of writing down all the terms explicitly they are taken into account by inhomogeneous broadening of individual resonant lines. Anisotropy of g-tensors in the treated systems is small, so effective g-factors of each radical can be evaluated as

$$g_i = g_{iXX}\sin^2\theta\cos^2\phi + g_{iYY}\sin^2\theta\sin^2\phi + g_{iZZ}\cos^2\theta, \quad (2)$$

where g_{XX}, g_{YY}, g_{ZZ} are principal values of corresponding g-tensor and polar and azimuthal angles θ, ϕ define an spatial orientation of g-tensor.

It is convenient to express equations in terms of angular frequency. Then Hamiltonian (1) in the rotating frame can be written as

$$\mathcal{H} = \omega_A S_{Az} + \omega_B S_{Bz} + J(\mathbf{S}_A \cdot \mathbf{S}_B) + \frac{D}{2}(3\cos^2\theta_D - 1)\left(S_z^2 - \frac{1}{3}\mathbf{S}^2\right). \quad (3)$$

Here $\omega_i = (g_i/g - 1)\omega + \Delta\omega_i$, where ω is a spectrometer microwave frequency, g_i is calculated using (2) and resonant g-factor g is defined by condition of resonance $g\mu B_0 = \omega$. The term $\Delta\omega_i$ corresponds to spreading of Larmor frequency within inhomogeneously broadened EPR line of a radical. It is supposed that other quantities in (3) are also evaluated in angular frequency units.

Calculations can be performed with convenience in basis set which is a direct product of two spin $S = \frac{1}{2}$ basis sets, i.e. $|\alpha\alpha\rangle$, $|\alpha\beta\rangle$, $|\beta\alpha\rangle$ and $|\beta\beta\rangle$. Spin operators for two-spin system in this basis can be easily obtained as Kronecker product of corresponding one-spin operators.

CTS which can be observed in the experiment is a weekly coupled secondary RP_2 formed from strongly coupled primary precursor RP_1 by sequential electron transfer as shown on the scheme Fig. 1(a). On the Fig. 1(a) k_Q is the rate of formation of the secondary pair RP_2, parameters j_1, Q_1 and j_2, Q_2 are the parameters controlling frequencies of singlet-triplet interconversion within RP_1 and RP_2. For both pairs $2Q_k$ is the difference of resonant frequencies ω_A and ω_B of two radicals, j_k arises from exchange and dipolar interactions [22].

It is important to note that saying "weakly coupled RP" we imply the case when $|\omega_A - \omega_B| \gg J, D$. For "strongly coupled RP" the inverse condition $|\omega_A - \omega_B| \ll J, D$ is fulfilled.

Since primary pair RP_1 is formed from photoexcited molecular singlet it has antiphase, or multiplet, polarization. Polarization of observable weakly coupled pair RP_2 may differ from polarization of RP_1 owing to prior evolution of its spin state: if parameter j_1 for primary RP_1 and formation rate k_Q are comparable, initial spin state of RP_1 has enough time to evolve.

We will split polarization and density matrix of secondary pair RP_2 into two conceivable contributions. For the sake of simplicity these two contributions will be treated separately. Such separation is allowed as far as density matrix obeys linear equation of motion, but actually there are no differently polarized observable pairs RP_2, and polarization of RP_2 is a composition of these two contributions.

The first contribution to density matrix of RP_2 originates from spin-correlated state of primary precursor, i.e. pure singlet $\rho_0^S = |S\rangle\langle S|$. As $S\rangle = (|\alpha\beta\rangle - |\beta\alpha\rangle)/\sqrt{2}$, density matrix ρ_0^S is given by

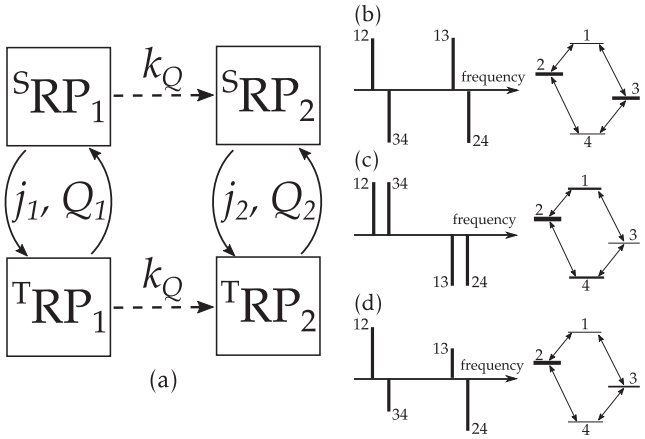

Fig. 1. The scheme (a) illustrates formation of secondary radical pair RP_2 from primary RP_1 by sequential electron transfer. As far as primary RP_1 is formed from photoexcited molecular singlet the polarization it transmits to its descendant RP_2 is antiphase (or multiplet) (b). Additional AE-polarization (c) is generated during electron transfer and contributes to polarization of observable RP_2 (d). Thereby polarization of RP_2 (d) is a composition of antiphase (b) and AE-polarization (c). Each stick spectrum shown here is illustrated by corresponding energy levels diagram, transitions are labeled accordingly. Population of each energy level is represented by its thickness. Assumption of weak coupling limit is fulfilled for the spectra (b–d).

$$\rho_0^S = \begin{pmatrix} 0 & & & \\ & 1/2 & -1/2 & \\ & -1/2 & 1/2 & \\ & & & 0 \end{pmatrix}. \tag{4}$$

Further in this work RPs having initial spin state ρ_0^S and, therefore, carrying antiphase polarization Fig. 1(b), will be called singlet-born RPs for short. Here lower index notation specifies time moment of density matrix evolution. It is important to understand that zero time moment does not coincide with actual start of the experiment, i.e. the beginning of laser pulse. In our treatment zero time is the moment of secondary RPs formation when their spin state is already prepared. Anyway, knowledge of exact moment of RP_2 formation is not critical for our treatment since we assume $k_Q^{-1} \ll T_{\text{daf}}$, where T_{daf} is a delay after laser flash, i.e. time gap between photoexcitation and microwave pulse sequence.

In the case of very fast electron transfer, when $k_Q \gg j_1, Q_1$, density matrix ρ_0^S exactly describes spin state and polarization of observable pairs RP_2. Under this assumption the conventional SCRP model is valid and polarization of RP_2 is pure antiphase.

On the other side, when charge separation and ST_0-mixing rates are comparable, polarization of observable RPs is not antiphase anymore. Treating this case we assume that AE-polarization shown on Fig. 1(c) is another contribution to total polarization of RP_2. Since each radical in AE-polarized RP carries net polarization and one radical is polarized oppositely to another, contribution to initial density matrix of RP_2 can be represented as $\rho_0^{AE} = S_{Bz} - S_{Az}$, or more specifically:

$$\rho_0^{AE} = \begin{pmatrix} 0 & & & \\ & -1 & & \\ & & 1 & \\ & & & 0 \end{pmatrix}. \tag{5}$$

We imply that ρ_0^{AE} represents an additional polarization which is generated during initial steps of charge separation. Thus overall initial density matrix of RP_2 is a weighted composition of two contributions ρ_0^S (singlet-born SCRP) and ρ_0^{AE} (AE-polarized RP):

$$\rho_0 = \rho_0^S + b\rho_0^{AE} \tag{6}$$

It is important to note that at the time of observation there is still non-zero magnetic interaction between radicals in RP_2 pair. Initial polarization of observable pair RP_2 corresponding to ρ_0 is shown on Fig. 1(d).

The polarization pattern shown on Fig. 1(d) seems to represent the most general situation taking place for RP formed as a result of sequential electron transfer. For the first time it was predicted in work [23]. Such type of EPR spectrum appears when both mechanisms of spin polarization, namely SCRP and CIDEP, act together. The work [22] also predicts formation of the polarization Fig. 1 (d) according to kinetic model of electron transfer similar to shown above on Fig. 1(a). Both works [22,23] give an explanation how mixed polarization pattern Fig. 1(d) can appear in experiment. In the present work we are not interested in actual intensities of RP_2 EPR lines or exact amount of AE-polarization has been generated (coefficient b in Eq. (6)). The aim is to examine how additional, with respect to antiphase, AE-polarization will manifest itself in ESE experiments.

If spin relaxation is omitted, density matrix of the spin system at certain time can be evaluated by series of unitary transformations with propagator $U_t = \exp(-i\mathcal{H}t)$ and thereby

$$\rho_{T+t} = U_t \rho_T U_t^{\dagger}.$$

During the application of a microwave pulse with oscillating magnetic field B_p the Hamiltonian (3) contains additional term $\omega_p S_x$ wherein $\omega_p = \frac{1}{2}(g_A + g_B)\mu B_p$ with high enough accuracy. Thus the evolution of the density matrix during the pulse of duration t_p is governed by operator $P(t_p, \xi) = \exp(-i\mathcal{H}t_p - iS_x\xi)$ where flip angle $\xi = \omega_p t_p$ is introduced.

Time dependence of magnetization is computed from corresponding evolution of the density matrix in conventional way. For polyoriented ensemble this dependence should be averaged over the spatial orientations of g-tensors according to (2), over angle θ_D which defines orientation of a whole radical pair and, finally, over shifts of Larmor frequencies $\Delta\omega_i$ caused by unresolved hyperfine interactions. Also since the system under study is considerably disordered distribution of dipole interaction values D should be taken into account. We suppose that all distributions are uncorrelated, g-tensor orientations of $P3HT^+$ and $PCBM^-$ are uncorrelated as well.

Averaging can be effectively performed by Monte-Carlo method. Usually number of simulations 10^6–10^7 per one data point is enough for good accuracy. Computational program was written on C++ using Intel MKL and Armadillo [24] libraries for matrix operations.

3. Results and discussion

In this section we will discuss the results of theoretical calculations in relation to temporal shape of ESE signal in P3HT/PCBM blends and ESEEM experiments. In two-pulse experiments, which are considered below, a microwave pulse sequence is applied to radicals generated by laser with delay after flash $T_{\text{daf}} = 1\mu s$ if it is not stated otherwise.

3.1. Validation of magnetic parameters of $P3HT^+$ and $PCBM^-$

Typical X-band EPR absorption spectrum of thermalized noninteracting radicals in P3HT/PCBM blend is shown on Fig. 2. The spectrum is calculated using g-tensor principal values taken from work [25] (see Table 1).

To take into account inhomogeneous broadening Gaussian shape of individual resonant line is assumed. Half-height width of lines is set equal to 3.5 MHz for both radicals. The model EPR absorption spectrum resulted from this choice of inhomogeneous

line width is shown on Fig. 2, panel B. The model spectrum approximates experimental EPR spectrum well enough, little difference between them is caused by g-strain effect [25], which is not included in our calculations. As can be seen from Fig. 2 at spectral lines of two radicals slightly overlap. However they are far enough to produce separate peaks.

3.2. Dependence of ESE signal on flip angle of the first microwave pulse

Spin-correlated RPs ($\rho_0 = \rho_0^S$) behave differently from thermalized spin system when flip angles in pulse sequence are varied. In the limit of weakly coupled RPs intensity of out-of-phase spin echo depends on flip angle of first pulse as follows [21]:

$$M_x \sim \sin 2\xi_1. \tag{7}$$

In derivation of Eq. (7) flip angle of second pulse is fixed $\xi_2 = \pi$ and single point detection of an echo signal at time $t = \tau$ after second pulse is assumed. Comparison of analytical dependence Eq. (7) with calculated echo intensity is shown on Fig. 3. As one can see from Fig. 3 calculated dependence is in good agreement with Eq. (7). Small deviation for angles greater than $\pi/2$ can be explained by contribution to ESE signal from RPs which don't satisfy the condition of weak coupling. Indeed, since EPR spectra of $P3HT^+$ and $PCBM^-$ partially overlap (see Fig. 2(B)) it is expected that even the case of strong coupling may be realized for small amount of radical pairs. Nevertheless the pulse sequence $\pi/4 - \tau - \pi$ is very close to optimal for out-of-phase echo detection in agreement with Eq. (7).

3.3. Echo signal modulation and ESEEM experiment

The echo signal of SCRP ($\rho_0 = \rho_0^S$) is known to be modulated when pulse spacing τ is varied. There is analytic expression [21] for modulation frequency ω_{mod}:

$$\omega_{\text{mod}}(\theta_D) = J - \frac{2}{3}D(3\cos^2\theta_D - 1), \tag{8}$$

and in polyoriented system out-of-phase echo at time $t = \tau$ after the second pulse is given by formula

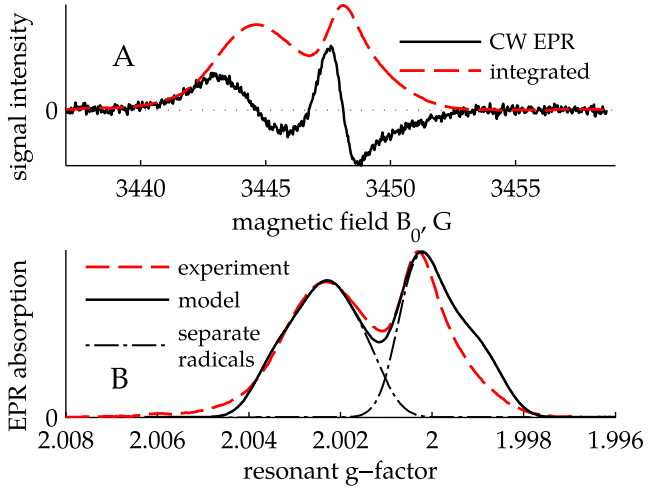

Fig. 2. Comparison of experimental and model EPR absorption spectrum. A: experimental X-band CW EPR spectrum of P3HT/PCBM composite under continuous illumination (solid black line). Its integral represents EPR absorption spectrum (dashed red line). B: calculated EPR absorption spectrum of thermalized $P3HT^+$ and $PCBM^-$ radicals (solid black line) and experimental EPR spectrum (dashed red line, the same data set as in panel A). Principal values of g-tensor shown in Table 1 were used to calculate the model spectrum. Dash-dotted black lines denote spectral lines of separate radicals. Temperature was 65 K, the microwave power was low enough to avoid signal saturation. Modulation amplitude was 1 G. (For interpretation of the references to color in this figure legend, the reader is referred to the web version of this article.)

Table 1
Principal values of g-tensor of radicals $P3HT^+$ and $PCBM^-$. Values were taken from [25].

	$P3HT^+$	$PCBM^-$
g_{XX}	2.00380	2.00058
g_{YY}	2.00230	2.00045
g_{ZZ}	2.00110	1.99845

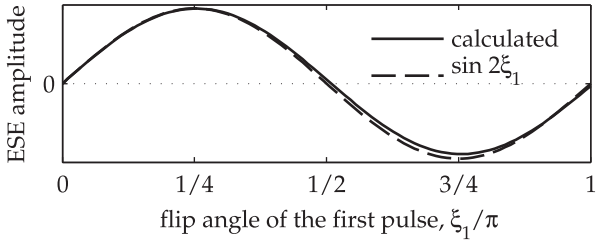

Fig. 3. Dependence of calculated out-of-phase echo amplitude (solid line) on flip angle ξ_1 of first microwave pulse for $P3HT^+/PCBM^-$ SCRP. Resonant g-factor is $g = 2.0011$ (center of the spectrum), value of dipole interaction 4 MHz is used. Pulse sequence is $\xi_1 - \tau - \pi$ where pulses of duration 4–16 ns are applied, pulse spacing $\tau = 0.46$ μs. ESE signal was integrated with integration window of 60 ns width centered on moment τ after the second pulse. Dashed line illustrates the deviation of calculated dependence from theoretical one.

$$M_x(\tau) \sim \int_0^{\pi} \sin\omega_{\text{mod}}\tau \sin\theta_D \mathrm{d}\theta_D.$$

In conventional two-pulse ESEEM experiment, echo is monitored at time $t = \tau$ (or the point of its maximum) while interpulse gap τ is increased. Such experiment provides an important information about magnitudes of interspin interactions and distances.

Unfortunately, when echo signal is weak single-point detection leads to a quite noisy ESEEM data. To improve signal-to-noise ratio one should somehow integrate echo signal in time-domain. It is possible to distort ESEEM trace upon integration [26], so the question is how to integrate an echo signal for good S/N ratio and avoid distortions at the same time.

The Fig. 4 shows dependence of out-of-phase echo signal on τ. Here pulse sequence $\pi/4 - \tau - \pi$ is used with nonselective pulses of 4 ns and 16 ns. In this paragraph we assume magnitude of dipole interaction is fixed and equal to 4 MHz, which corresponds with interspin distance $r \approx 2.7$ nm. While interspin distance disorder is left aside, averaging over directions of interspin vector is included here. Exchange interaction is ignored.

The Fig. 4 illustrates that out-of-phase ESE signal is modulated and its shape changes dramatically when τ is varied. In in-phase channel small signal can be observed which vanishes at moment $t = \tau$ after the end of the second pulse [27]. Dependence of the ESE on τ results in out-of-phase ESEEM traces shown on Fig. 5.

Solid red line in Fig. 5 depicts ESEEM produced as a result of conventional approach mentioned above (single-point detection) and serves as the reference trace. Dashed black line corresponds to the result of echo integration by gate length 60 ns with integration window centered at time $t = \tau$ after 2nd pulse. When echo signal shape is nearly bell-like (see e.g. black line in Fig. 4) this choice of integration window is close to half-height integration. For simplicity, since pulses are sufficiently short we don't make any difference between $t = \tau$ and the moment of signal maximum.

As can be seen from Fig. 5, reference ESEEM trace (red line) and the one derived from echo integration (black line) agree within their amplitudes. Thus signal intensity as well as signal-to-noise ratio in an experiment can be enhanced safely if integration window is centered at time $t = \tau$ after the end of the second pulse.

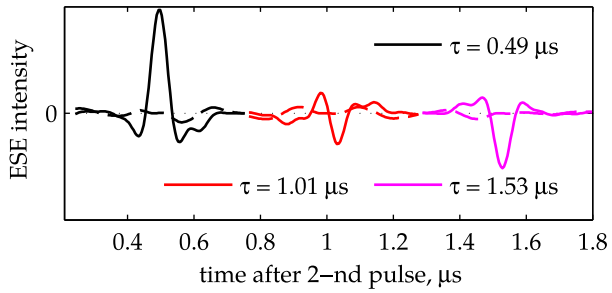

Fig. 4. Spin echo shape dependence on pulse spacing τ. Resonant g-factor is $g = 2.0011$ (spectrum center), value of dipole interaction $D = 4$ MHz is used. Pulse sequence is $\pi/4 - \tau - \pi$ where pulses of duration 4–16 ns are applied. Out-of-phase part of the echo is represented by solid lines, dashed lines denote in-phase part.

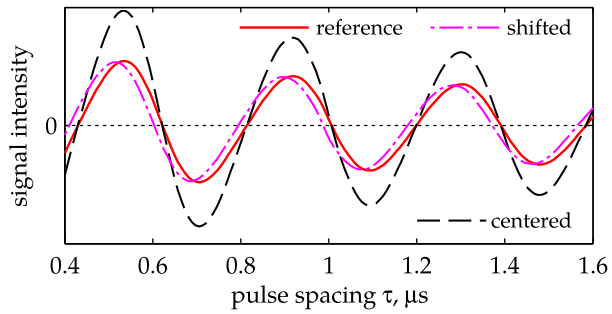

Fig. 5. Comparison of out-of-phase ESEEM traces resulted from different ways of echo integration. Solid red line, marked as reference, is echo signal detected at single time point $t = \tau$ after 2nd pulse. For the purpose of legibility it was increased by factor of $\times 5$. ESEEM trace represented by dashed black line is the result of echo integration over interval of 60 ns length, which is centered on the point the reference trace is observed at, i.e. at time $t = \tau$. And, finally, if integration interval is shifted and not centered on $t = \tau$, the whole ESEEM trace shifts as indicated by magenta dash-dotted line. In this example the integration interval is centered at time $t = \tau + 30$ ns. Pulse sequence and other conditions are the same as for Fig. 4. (For interpretation of the references to color in this figure legend, the reader is referred to the web version of this article.)

If integration window is not centered at $t = \tau$, ESEEM trace is shifted in time with respect to the reference. This is illustrated by magenta dash-dotted line in Fig. 5. Here gate length is the same as in previous case, but the whole integration interval is shifted by 30 ns to greater times so that it is centered on $t = \tau + 30$ ns now. This leads to time offset of the ESEEM signal. In other words, signal derived from such integration is time-shifted in relation to reference which is detected at $t = \tau$.

Because of intrinsic disorder of bulk-heterojunction blends the magnitude of dipolar coupling between constituents of P3HT/PCBM radical pairs is appreciably distributed. Even though we are not taking into account this distribution here, the general conclusion of this section remains valid for real composite as well. Indeed, experimental ESEEM trace can be distorted upon echo integration similarly to its individual components corresponding to certain dipolar coupling.

3.4. Influence of interspin distance distribution

In order to take into account interspin distance disorder, which was left aside until now, ESE signals were averaged over model density distribution function $G(r)$ shown on Fig. 6. This probability density function is analogous to function introduced in [18] and consists of two halved Gaussian distributions with shared center but different half-height widths. The exact parameters of $G(r)$ are pointed out in caption of the Fig. 6.

As far as we use approximation of point dipoles the connection between interspin distance r and magnitude of dipole interaction is given by

$$D/\mathrm{MHz} = -\frac{77.8}{(r/\mathrm{nm})^3}. \tag{9}$$

Mean value of dipole interaction magnitude calculated using (9) and the chosen distribution of interspin distances is $\langle D \rangle = -1.33$ MHz.

The calculated ESE signals of singlet-born RPs ($\rho_0 = \rho_0^S$) with interspin distance distribution taken into account are presented on Fig. 7 for two different spectral positions. In this paragraph we use value $T_{\mathrm{daf}} = 300$ ns. Out-of-phase echo component has nearly bell-like shape with small wings at both ends at any spectral position. Also the shape does not change upon variation of interpulse gap τ (not shown), being in sharp contrast to Fig. 4.

Evolution of out-of-phase ESE intensity as function of τ is shown on Fig. 8. Echo signal was integrated with integration interval of 60 ns length, centered as explained in previous section. The calculations are performed at different values of resonant g-factors. As one can see these ESEEM traces are independent of spectral position: they differ only in amplitudes. Solid red line presents ESEEM trace averaged over the whole EPR spectrum. We conclude that choice of spectral position during an experiment does not affect on ESEEM signal of singlet-born $P3HT^+/PCBM^-$ radical pairs.

Out-of-phase echo and ESEEM of singlet-born RPs as function of excitation bandwidth are examined in SI.

3.5. Echo shape and ESEEM of AE-polarized radical pairs

Now we consider ESE time-domain shape and ESEEM of $P3HT^+/PCBM^-$ radical pairs with initial state $\rho_0 = \rho_0^{AE}$. It is remarkable that along with singlet-born SCRP AE-polarized RP is an another case when significant out-of-phase ESE signal arises.

Additional AE-polarization of radical pairs leads to ESE signals which are shown on Fig. 9. Distribution of interspin distances is also taken into account here in the same way as in previous section (see Fig. 6).

Out-of-phase echo shape shown on Fig. 9 has nearly symmetric positive and negative parts, but however it yields nonzero signal upon integration. The integrated echo as function of pulse spacing τ is presented on Fig. 10. Two cases are shown: ESEEM trace of radical pairs when interspin distance is fixed ($r = 2.7$ nm) and the trace of disordered system. Unlike ESEEM trace of singlet-born radical pairs, echo decay presented on Fig. 10 tends to be nonzero when $\tau = 0$. Moreover, ESEEM signal of AE-polarized RPs, being averaged over distribution of interspin distances, decreases much faster than signal of singlet-born pairs.

Another difference is behavior of ESEEM traces when resonant position in the spectrum is varied. As was shown in previous part,

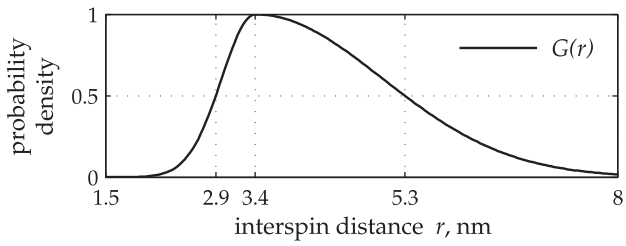

Fig. 6. Model probability density function of interspin distances in $P3HT^+/PCBM^-$ radical pair. $G(r) \sim \exp\left((r - r_0)^2/a^2\right)$ when $r \leqslant r_0$ and $G(r) \sim \exp\left((r - r_0)^2/b^2\right)$ otherwise. The most probable interspin distance is $r_0 = 3.4$ nm, half-height widths of left and right sides of distribution are 1.0 nm and 3.8 nm respectively.

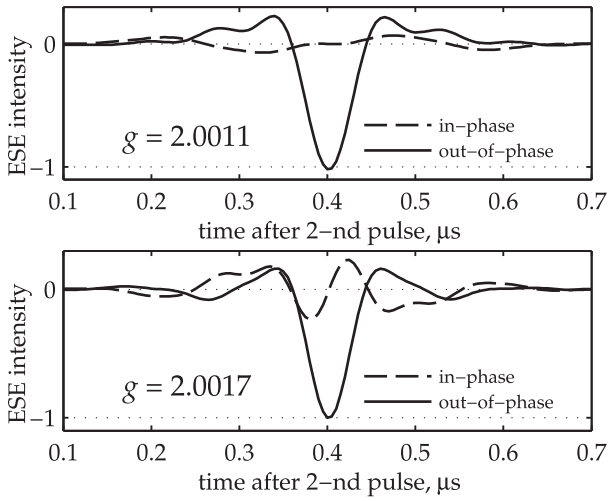

Fig. 7. Time-domain ESE signal of singlet-born RP P3HT$^+$/PCBM$^-$ after averaging over model distribution of interspin distances. Pulse sequence is $\pi/4 - \tau - \pi$ where pulses of duration 4–16 ns are applied, interpulse gap is $\tau = 400$ ns. Upper and lower panes show echo signals obtained at different points of EPR spectrum: spectrum center (resonant $g = 2.0011$) and P3HT$^+$ radical (resonant $g = 2.0017$) respectively.

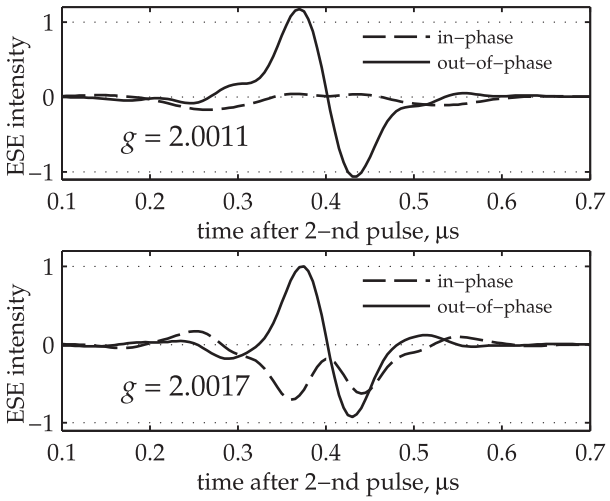

Fig. 9. Time-domain ESE signal of AE-polarized P3HT$^+$/PCBM$^-$ radical pairs with interspin distance distribution taken into account. Pulse sequence is $\pi/4 - \tau - \pi$ where pulses of duration 4–16 ns are applied, interpulse gap is $\tau = 400$ ns. Upper and lower panes show echo signals obtained at different points of EPR spectrum: spectrum center (resonant $g = 2.0011$) and P3HT$^+$ radical (resonant $g = 2.0017$) respectively.

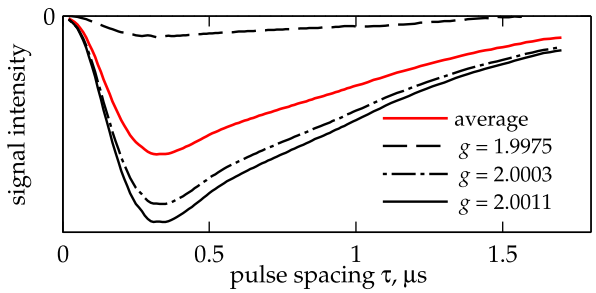

Fig. 8. Out-of-phase ESEEM signal of singlet-born RP P3HT$^+$/PCBM$^-$ with interspin distance distribution taken into account. Traces calculated at different spectral positions are presented (black lines) and averaged (red line) over them. Integration window is 60 ns width and centered on moment $t = \tau$ after the end of the second pulse. (For interpretation of the references to color in this figure legend, the reader is referred to the web version of this article.)

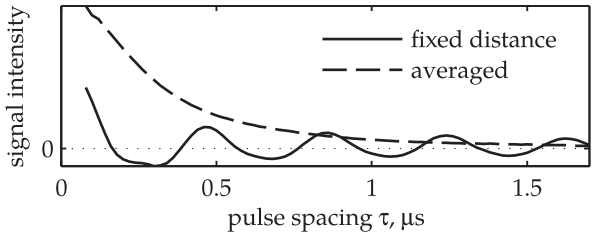

Fig. 10. Out-of-phase ESEEM signal of AE-polarized P3HT$^+$/PCBM$^-$ radical pair. Solid line presents ESEEM trace of ensemble of pairs with fixed interspin distance ($r = 2.7$ nm, $D = 4.0$ MHz). Dashed line shows the result of averaging traces with certain interspin distance over model distance distribution shown on Fig. 6. Integration window is 60 ns width and centered on moment $t = \tau$ after the end of second pulse. The traces were calculated at the center of EPR spectrum (resonant $g = 2.0011$).

out-of-phase ESEEM traces of singlet-born pairs are independent on spectral position. On the other hand, sign of ESEEM trace depends on resonant point in the case of AE-polarized RP. Fig. 11 illustrates ESEEM traces of AE-polarized radical pairs as function of resonant spectral position. Thick dash-dotted line is the ESEEM trace averaged over a number of resonant positions across the whole EPR spectrum. As one can see different ESEEM traces interfere destructively and average trace is close to zero. Thus in any ESEEM experiment on spin-correlated RPs one can exclude component of echo decay caused by additional AE-polarization by measuring ESEEM traces at different spectral positions and subsequent averaging over the whole EPR spectrum. In particular, average trace shown on the Fig. 11 is a superposition of traces calculated at 15 resonant points which are evenly spaced in the interval covering the whole EPR spectrum from low-field ($g = 2.0045$) to high-field ($g = 1.9975$) edge.

Also it is important to note that, especially in case of AE-polarized RPs, microwave pulses produce intensive free induction decay (FID) signal which obstructs a proper echo detection when τ is small. Therefore it is necessary to use a phase-cycling technique to overcome FID influence. The simplest technique is to detect signal twice with different signs of the last microwave pulse

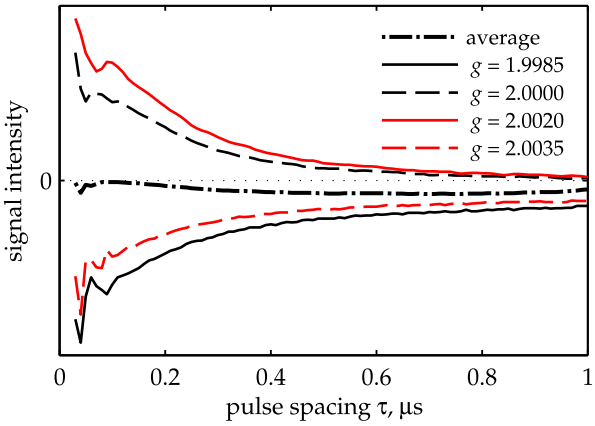

Fig. 11. Dependence of out-of-phase ESEEM traces on spectral position for AE-polarized RPs in disordered system (interspin distance distribution is shown on Fig. 6). The traces were computed for 15 different positions across the whole EPR spectrum and some of them are shown. The trace averaged over all spectral positions is presented by dash-dotted line. Echo was integrated over interval of 60 ns length, centered at time $t = \tau$ after the end of second pulse.

(namely, changing rotation angle $\xi = \pi$ to $\xi = -\pi$) and to sum results after. Such technique was used to calculate echo signals in this section.

Echo shape and ESEEM of AE-polarized RPs as function of excitation bandwidth are examined in SI.

3.6. Experiment: time-domain echo shape and ESEEM

Experimental time-domain ESE shape of $P3HT^+/PCBM^-$ radical pairs is shown on Fig. 12. The experiment was performed at temperature of 65 K and at magnetic field of 3446 G strength, which corresponds to g-factor $g = 2.0017$. Echo signal measured at $T_{daf} = 99$ ms is considered as a background signal originated from thermalized noninteracting spins of $P3HT^+$ and $PCBM^-$ or other long-living radicals, such as permanent defects due to continuous irradiation. This background signal is subtracted from the data for $T_{daf} = 280$ ns to extract weak signal of CT state. The sample was irradiated by Nd:YAG laser with a wavelength of 532 nm, short repetition rate of 10 Hz and pulse power of 0.6 mJ approximately. Other experimental conditions are the same as in [18].

The out-of-phase echo shape observed in experiment differs significantly from bell-like shapes shown on Fig. 7, but it is similar to echo shape of AE-polarized RPs. Either as the echo signal shown on Fig. 9, out-of-phase component of experimental echo signal has almost symmetrical negative and positive parts. Probable explanation of such time-domain echo shape is that it is predominantly defined by AE component of total RP_2 polarization. In other words, signal arising from antiphase component is masked by huge signal of AE-polarization.

ESEEM experiment provide another proof that polarization of observable RPs is a composition of antiphase and AE parts. To obtain ESE amplitude as function of τ echo signals were measured separately for different τ values and then numerically integrated. The echo signal presented on Fig. 12 belongs to this series of measurements. Integration window was 60 ns width and centered on the time point where out-of-phase echo signal is equal to zero. Peak-to-peak width for out-of-phase ESE is also 60 ns. The result is shown in Fig. 13 (panel B).

Panel A of Fig. 13 shows superposition (solid red line) of ESE decays originated from singlet-born (dash-dotted line) and AE-polarized (dashed line) RPs. This ESEEM signal, obtained as a superposition with $b = 1$ (see Eq. (6)), is in a good qualitative agreement with the experiment. Thus experimental out-of-phase ESEEM signal can be divided into two parts which have different origin. The part arising from additional AE-polarization can be suppressed by averaging over resonant positions across the whole EPR spectrum of RP, as it is shown by our calculations.

Reliability of an ESEEM experiments, especially when time-domain echo shape is close to antisymmetric, higly depends on stability and tuning accuracy of microwave detection phase. The ESEEM trace of the background signal (black dashed line on Fig. 13(B)) serves as a reference for controlling the phasing. See SI for more details.

Importantly, when polarization of observable RP_2 contains significant AE component, sine Fourier transform of out-of-phase ESEEM does not result in distribution of dipolar frequencies (Pake doublet).

Previously, in a number of works, for instance [6,9,28], it was reported that polarization of $P3HT^+/PCBM^-$ RPs is solely formed by singlet SCRP mechanism. This conclusion is mostly based on time-resolved EPR spectra revealing specific polarization pattern EAEA, which is generally associated with SCRP. Indeed, the polarization produced by SCRP mechanism, antiphase polarization, accords with this specific pattern, but it is not the only one possible. Also EAEA polarization pattern can be reproduced by mixed polarization (see Fig. 1d), which we believe the actual polarization $P3HT^+/PCBM^-$ RPs have. Time-resolved EPR experiments are just not able to distinguish purely antiphase and mixed polarizations. In other words, it is very hard to tell whether a TREPR spectrum is purely antiphase or it contains A/E polarization component, especially in the case of such disordered systems like P3HT/PCBM blend.

Even though experimental TR EPR spectra were simulated with good agreement [5], the simulation was based on questionable assumptions and contained too many parameters of fitting. Therefore, it cannot be considered as *irrefutable* evidence for singlet SCRP theory. Instead, in the present work we offer a simple hypothesis, which is not only able to reproduce previous TR EPR experiments, but also covers ESE experiments as well.

Summarizing, our results do not contradict any known experimental results, including time-resolved EPR data.

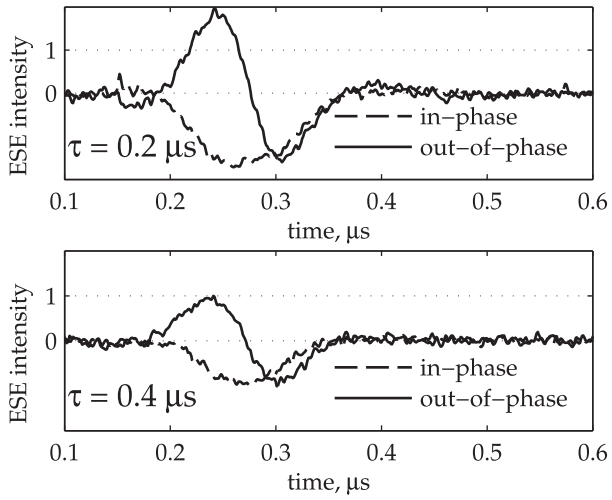

Fig. 12. In-phase and out-of-phase echo signal of $P3HT^+/PCBM^-$ radical pairs (experiment). The shapes obtained by subtraction of measurements with $T_{daf} = 280$ ns and $T_{daf} = 99$ ms. Two-pulse sequence with nonselective pulses was used with pulse gap $\tau = 0.2$ μs and $\tau = 0.4$ μs (upper and lower panel respectively). Temperature was 65 K, resonant spectral position is $g = 2.0017$ ($P3HT^+$ radical).

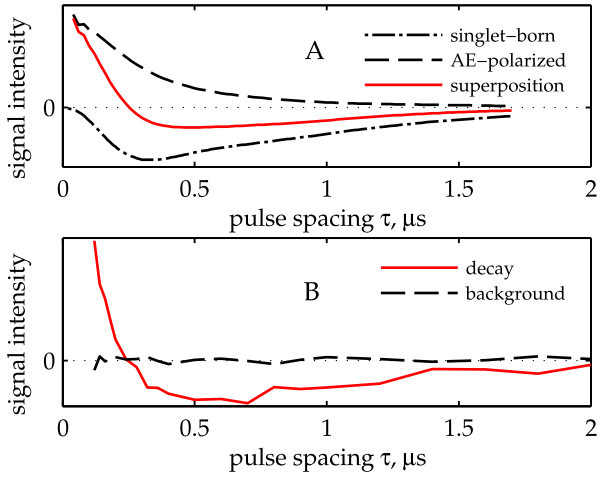

Fig. 13. Comparison of calculated out-of-phase ESE decay with experimentally observed one. Panel A: ESEEM signal of singlet-born RPs (dash-dotted line), ESEEM signal of AE-polarized RPs (dashed line), and their superposition (solid line). Panel B: experimentally observed ESE decay (solid line) and reference background signal measured at $T_{daf} = 99$ ms (dashed line). Spectral position is $g = 2.0017$ ($P3HT^+$ radical).

4. Conclusion

We have investigated electron spin echo temporal shape of spin-correlated radical pairs in P3HT/PCBM blends in relation to electron spin echo envelope modulation experiments.

Out-of-phase electron spin echo intensity of spin-correlated radical pairs depends on flip angle of first pulse and for sufficiently short pulses this dependence accords fine with analytical dependence. The turning angle of first pulse $\xi_1 = \pi/4$ is close to optimal for out-of-phase electron spin echo detection. For accurate results it is important to avoid distortion of an ESEEM trace upon an echo integration. When echo integration window is centered at time $t = \tau$ after the second pulse distortions are minimal and they are significant otherwise.

Interspin distance distribution in $P3HT^{+}/PCBM^{-}$ radical pairs was taken into account by averaging of calculated time-domain ESE signals over model probability density function.

Comparison of these computations with experiment revealed that experimental results cannot be reproduced without assuming additional, besides purely singlet, component contributing to initial spin state of observable RPs. This component, named AE-polarization, is produced as result of spin state evolution at early steps of sequential electron transfer. Such assumption gives convincing agreement with an experiment, both time-domain ESE and ESEEM.

Experimentally observed ESEEM signal, being a superposition, includes two parts originated from two different components of observable RP polarization, namely antiphase and AE-polarization. Thus it cannot be interpreted directly within singlet SCRP model. However the second component can be suppressed by averaging over resonant positions across the whole EPR spectrum.

From this new point of view results of work [18] should be revised. Owing to almost antisymmetric echo shape of AE-polarized RPs their ESEEM signal intensity depends drastically on integration gate: gates shorter than peak-to-peak echo width lead to result close to zero, but integration with longer gates produces strong signal. In work [18] almost the whole ESE signal was integrated, and ESEEM component corresponding to antiphase part of polarization, which is relatively weak, was hidden. Thus interpretation of ESE decay given on [18] should be corrected. This work is in progress now. The more recent results are available in [19].

The next step is determination of how far from pure singlet actual polarization is. Exact amount of additional AE-polarization depends on kinetic constants of charge separation and recombination, which in turn determine spin evolution of RP at the very beginning of overall charge separation process, inaccessible to EPR methods directly. However, pulsed ESE techniques, in conjunction with numerical simulations, can be employed to measure contribution of additional polarization and, thus, to determine kinetic constants mentioned above. This information is critical for development of detailed theory of charge separation in OPV devices.

Acknowledgments

This work was supported by the Russian Foundation for Basic Research: Grants 15-33-20421 and 15-03-07682; the Ministry of Education and Science of the Russian Federation; Alexander von Humboldt Foundation in frame of research group linkage project “Light-induced processes and paramagnetic species in organic photovoltaics and photosynthesis”.

Appendix A. Supplementary material

Supplementary data associated with this article can be found, in the online version, at http://dx.doi.org/10.1016/j.jmr.2017.01.016.

References

[1] G. Dennler, K. Forberich, M.C. Scharber, C.J. Brabec, I. Tomiš, K. Hingerl, T. Fromherz, Angle dependence of external and internal quantum efficiencies in bulk-heterojunction organic solar cells, J. Appl. Phys. 102 (2007) 1–7, http://dx.doi.org/10.1063/1.2777724.

[2] J. Jo, S.I. Na, S.S. Kim, T.W. Lee, Y. Chung, S.J. Kang, D. Vak, D.Y. Kim, J. Jang, N. Seok-In, K. Seok-Soon, L. Tae-Woo, C. Youngsu, K. Seok-Ju, V. Doojin, K. Dong-Yu, Three-dimensional bulk heterojunction morphology for achieving high internal quantum efficiency in polymer solar cells, Adv. Funct. Mater. 19 (2009) 2398–2406, http://dx.doi.org/10.1002/adfm.200900183.

[3] S. Few, J.M. Frost, J. Nelson, Models of charge pair generation in organic solar cells, Phys. Chem. Chem. Phys. 17 (2014) 2311–2325, http://dx.doi.org/10.1039/C4CP03663H. <http://pubs.rsc.org/en/Content/ArticleLanding/2014/CP/C4CP03663H>.

[4] F. Gao, O. Inganäs, Charge generation in polymer-fullerene bulk-heterojunction solar cells, Phys. Chem. Chem. Phys. 16 (38) (2014) 20291–20304, http://dx.doi.org/10.1039/c4cp01814a. <http://www.ncbi.nlm.nih.gov/pubmed/24994122>.

[5] Y. Kobori, R. Noji, S. Tsuganezawa, Initial molecular photocurrent: Nanostructure and motion of weakly bound charge-separated state in organic photovoltaic interface, J. Phys. Chem. C 117 (2013) 1589–1599, http://dx.doi.org/10.1021/jp309421s.

[6] J. Behrends, A. Sperlich, A. Schnegg, T. Biskup, C. Teutloff, K. Lips, V. Dyakonov, R. Bittl, Direct detection of photoinduced charge transfer complexes in polymer fullerene blends, Phys. Rev. B 85 (12) (2012) 125206, http://dx.doi.org/10.1103/PhysRevB.85.125206. <http://link.aps.org/doi/10.1103/PhysRevB.85.125206>.

[7] F. Kraffert, R. Steyrleuthner, S. Albrecht, D. Neher, M.C. Scharber, R. Bittl, J. Behrends, Charge separation in PCPDTBT:PCBM blends from an EPR perspective, J. Phys. Chem. C 118 (2014) 28482–28493, http://dx.doi.org/10.1021/jp509650v. <http://pubs.acs.org/doi/abs/10.1021/jp509650v>.

[8] N.S. Sariciftci, L. Smilowitz, A.J. Heeger, F. Wudl, Photoinduced electron transfer from a conducting polymer to buckminsterfullerene, Science 258 (1992) 1474–1476, http://dx.doi.org/10.1126/science.258.5087.1474.

[9] L. Pasimeni, L. Franco, M. Ruzzi, A. Mucci, L. Schenetti, C. Luo, D.M. Guldi, K. Kordatos, M. Prato, Evidence of high charge mobility in photoirradiated polythiophenefullerene composites, J. Mater. Chem. 11 (4) (2001) 981–983, http://dx.doi.org/10.1039/b100842k. <http://xlink.rsc.org/?DOI=b100842k>.

[10] L. Pasimeni, M. Ruzzi, M. Prato, T. Da Ros, G. Barbarella, M. Zambianchi, Spin correlated radical ion pairs generated by photoinduced electron transfer in composites of sexithiophene/fullerene derivatives: a transient EPR study, Chem. Phys. 263 (1) (2001) 83–94, http://dx.doi.org/10.1016/S0301-0104(00)00339-6. <http://linkinghub.elsevier.com/retrieve/pii/S0301010400003396>.

[11] M.N. Uvarov, a.G. Popov, E.a. Lukina, L.V. Kulik, Spin relaxation and structure of light-induced spin-correlated $PCBM^{-}/P3HT^{+}$ radical pairs, J. Struct. Chem. 55 (4) (2014) 644–650, http://dx.doi.org/10.1134/S0022476614040088.

[12] S.A. Dzuba, P. Gast, A.J. Hoff, ESEEM study of spin-spin interactions in spin-polarised P+QA pairs in the photosynthetic purple bacterium Rhodobacter sphaeroides R26, Chem. Phys. Lett. 236 (6) (1995) 595–602, http://dx.doi.org/10.1016/0009-2614(95)00259-7. <http://linkinghub.elsevier.com/retrieve/pii/0009261495002597>.

[13] R. Bittl, S.G. Zech, Pulsed EPR study of spin-coupled radical pairs in photosynthetic reaction centers: measurement of the distance between P_{700}^{+} and A_1^{-} in photosystem I and between P_{865}^{+} and Q_A^{-} in bacterial reaction centers, J. Phys. Chem. B 101 (1997) 1429–1436, http://dx.doi.org/10.1021/jp962256q.

[14] C. Fursman, P. Hore, Distance determination in spin-correlated radical pairs in photosynthetic reaction centres by electron spin echo envelope modulation, Chem. Phys. Lett. 303 (5–6) (1999) 593–600, http://dx.doi.org/10.1016/S0009-2614(99)00185-2. <http://linkinghub.elsevier.com/retrieve/pii/S0009261499001852>.

[15] A. Savitsky, A.A. Dubinskii, M. Flores, W. Lubitz, K. Möbius, Orientation-resolving pulsed electron dipolar high-field EPR spectroscopy on disordered solids: I. Structure of spin-correlated radical pairs in bacterial photosynthetic reaction centers, J. Phys. Chem. B 111 (22) (2007) 6245–6262, http://dx.doi.org/10.1021/jp070016c, arXiv:1408.1149 <http://www.ncbi.nlm.nih.gov/pubmed/23642108>. <http://pubs.acs.org/doi/abs/10.1021/jp401573z>. <http://pubs.acs.org/doi/abs/10.1021/jp070016c>.

[16] R. Carmieli, Q. Mi, A.B. Ricks, E.M. Giacobbe, S.M. Mickley, M.R. Wasielewski, Direct measurement of photoinduced charge separation distances in donor-acceptor systems for artificial photosynthesis using OOP-ESEEM, J. Am. Chem. Soc. 131 (24) (2009) 8372–8373, http://dx.doi.org/10.1021/ja902864h. <http://www.ncbi.nlm.nih.gov/pubmed/19476357>.

[17] M.T. Colvin, R. Carmieli, T. Miura, S. Richert, D.M. Gardner, A.L. Smeigh, S.M. Dyar, S.M. Conron, M.a. Ratner, M.R. Wasielewski, Electron spin polarization transfer from photogenerated spin-correlated radical pairs to a stable radical observer spin, J. Phys. Chem. A 117 (25) (2013) 5314–5325, http://dx.doi.org/10.1021/jp4045012. <http://www.ncbi.nlm.nih.gov/pubmed/23721288>.

[18] E.A. Lukina, A.A. Popov, M.N. Uvarov, L.V. Kulik, Out-of-phase electron spin echo studies of light-induced charge-transfer states in P3HT/PCBM composite, J. Phys. Chem. B 119 (43) (2015) 13543–13548, http://dx.doi.org/10.1021/acs.jpcb.5b02142. <http://pubs.acs.org/doi/10.1021/acs.jpcb.5b02142>.

[19] E.A. Lukina, A.A. Popov, M.N. Uvarov, E.A. Suturina, E.J. Reijerse, L.V. Kulik, Light-induced charge separation in a P3HT/PC70BM composite as studied by out-of-phase electron spin echo spectroscopy, Phys. Chem. Chem. Phys. 18 (41) (2016) 28585–28593, http://dx.doi.org/10.1039/C6CP05389K. <http://pubs.rsc.org/en/Content/ArticleLanding/2016/CP/C6CP05389K>. <http://xlink.rsc.org/?DOI=C6CP05389K>.

[20] S.A. Dzuba, M.K. Bosch, A.J. Hoff, Electron spin echo detection of quantum beats and double-quantum coherence in spin-correlated radical pairs of protonated photosynthetic reaction centers, Chem. Phys. Lett. 248 (5–6) (1996) 427–433, http://dx.doi.org/10.1016/0009-2614(96)87702-5. <http://www.sciencedirect.com/science/article/pii/0009261496877025>. <http://linkinghub.elsevier.com/retrieve/pii/0009261496877025>.

[21] A.J. Hoff, P. Gast, S.A. Dzuba, C.R. Timmel, C.E. Fursman, P. Hore, The nuts and bolts of distance determination and zero- and double-quantum coherence in photoinduced radical pairs, Spectrochim. Acta Part A Mol. Biomol. Spectrosc. 54 (14) (1998) 2283–2293, http://dx.doi.org/10.1016/S1386-1425(98)00211-X. <http://linkinghub.elsevier.com/retrieve/pii/S138614259800211X>.

[22] P.J. Hore, Transfer of spin correlation between radical pairs in the initial steps of photosynthetic energy conversion, Mol. Phys. 89 (4) (1996) 1195–1202, http://dx.doi.org/10.1080/002689796173598. <http://www.tandfonline.com/doi/abs/10.1080/002689796173598>.

[23] J.R. Norris, A.L. Morris, M.C. Thurnauer, J. Tang, A general model of electron spin polarization arising from the interactions within radical pairs, J. Chem. Phys. 92 (7) (1990) 4239, http://dx.doi.org/10.1063/1.457782. <http://scitation.aip.org/content/aip/journal/jcp/92/7/10.1063/1.457782>.

[24] C. Sanderson, Armadillo: An Open Source C++ Linear Algebra Library for Fast Prototyping and Computationally Intensive Experiments, Tech. rep., NICTA, 2010.

[25] O.G. Poluektov, S. Filippone, N. Martín, A. Sperlich, C. Deibel, V. Dyakonov, Spin signatures of photogenerated radical anions in polymer-[70]fullerene bulk heterojunctions: high frequency pulsed EPR spectroscopy, J. Phys. Chem. B 114 (45) (2010) 14426–14429, http://dx.doi.org/10.1021/jp1012347, arXiv:1110.1577 <http://www.ncbi.nlm.nih.gov/pubmed/20392099>.

[26] A.V. Astashkin, V.V. Kozlyuk, A.M. Raitsimring, ESEEM measurements with time-resolved detection of the entire ESE signal shape, J. Magn. Reson. 145 (2) (2000) 357–363, http://dx.doi.org/10.1006/jmre.2000.2100.

[27] J. Tang, M.C. Thurnauer, J.R. Norris, Electron spin echo envelope modulation due to exchange and dipolar interactions in a spin-correlated radical pair, Chem. Phys. Lett. 219 (3–4) (1994) 283–290, http://dx.doi.org/10.1016/0009-2614(94)87059-4. <http://linkinghub.elsevier.com/retrieve/pii/0009261494870594>.

[28] J. Niklas, S. Beaupré, M. Leclerc, T. Xu, L. Yu, A. Sperlich, V. Dyakonov, O.G. Poluektov, Photoinduced dynamics of charge separation: from photosynthesis to polymerfullerene bulk heterojunctions, J. Phys. Chem. B 119 (24) (2015) 7407–7416, http://dx.doi.org/10.1021/jp511021v.